

A Metal Forming Analysis by Using the Hybrid PCM/FEM

Y.-M. Guo¹

Abstract: In this paper, for analyses of the rigid-plastic metal forming problems, a hybrid PCM/FEM is developed. By introducing a boundary layer of finite element in boundary domain of workpiece, unsatisfactory issue of the positivity conditions of boundary points can be avoided, and the complicated boundary conditions can be easily imposed with the boundary layer of finite element. A plane strain upsetting process is analyzed by using the hybrid PCM/FEM.

Keywords: Point collocation method, rigid-plastic FEM, moving least-square approximation, positivity conditions, metal forming.

1 Introduction

Meshless methods require no costly mesh generation and remeshing, and have found application in many references. The early representatives of meshless methods are the diffuse element method [Nayroles, Touzot, Villon (1992)], the element free Galerkin method [Belytschko, Lu, Gu (1994)], the reproducing kernel particle method [Liu et al. (1995)], the finite point method [Onate et al. (1996a)], the hp-clouds method [Duarte, Oden (1996)], the partition of unity method [Melenk, Babuska (1996)], the meshless local Petrov-Galerkin (MLPG) approach [Atluri, Zhu (1998)], the local boundary integral equation method [Zhu, Zhang, Atluri (1998)], and the point collocation method (PCM) based on reproducing kernel approximations [Aluru (2000)]. Some meshless methods are based on weak form, in which background meshes are inevitable in implementation to obtain the numerical integration. Some meshless methods are truly meshless methods, in which no background meshes are introduced. In most meshless techniques, however, complicated non-polynomial interpolation functions are used which render the integration of the weak form rather difficult. Failure to perform the integration accurately results in loss of accuracy and possibly stability of solution scheme. The integration of complicated non-polynomial interpolation function costs much CPU time, too.

¹ Kagoshima University, Kagoshima City, Japan

The PCM is a kind of truly meshless method, and has no issues of the integration scheme, the integration accuracy and the integration CPU time. Therefore, the PCM has some advantages such as no mesh, no integration. Several PCMs based on different types of approximations or interpolations have been presented in the literature. Aluru [Aluru (2000)] has presented a PCM based on reproducing kernel approximations for numerical solution partial differential equations with appropriate boundary conditions. Jin, Li and Aluru [Jin, Li, Aluru (2004)] have shown the robustness of collocation meshless methods can be improved by ensuring that the positivity conditions are satisfied when constructing approximation functions and their derivatives. Atluri, Liu and Han [Atluri, Liu, Han (2006a)] have presented a MLPG mixed collocation method by using the Dirac delta function as the test function in the MLPG method, and shown that the MPLG mixed collocation method is more efficient than the other MLPG implementations, including the MLPG finite volume method. Atluri, Liu and Han [Atluri, Liu, Han (2006b)] have proposed a finite difference method, within the framework of the MLPG approach, for solving solid mechanics problems. Wu, Shen and Tao [Wu, Shen, Tao (2007)] have used the MLPG collocation method to compute two-dimensional heat conduction problems in irregular domain. Li and Atluri [Li, Atluri (2008a)] have demonstrated the suitability and versatility of the MLPG mixed collocation method by solving the problem of topology-optimization of elastic structures. In addition, the MLPG mixed collocation method has also been successfully used in material orientation and topology optimization of anisotropic solids and structures [Li, Atluri (2008b)]. Chantasiriwan [Chantasiriwan (2006)] has provided results of using the multiquadric collocation method to solve the lid-driven cavity flow problem. Kosec and Sarler [Kosec, Sarler (2008)] have explored the application of the mesh-free local radial basis function collocation method in solution of coupled heat transfer and fluid flow problems in Darcy porous media. Onate et al. [Onate et al. (1996a)] have proposed a finite point method based on weighted least squares interpolations for the analyses of convective transport and fluid flow problems. Onate et al. [Onate et al. (1996b)] have also proposed a residual stabilization procedure, adequate for the finite point method, and further extended the finite point method to the solution of the advective-convective transport equations as well as those governing the flow of compressible fluids. Boroomand, Tabatabaei and Onate [Boroomand, Tabatabaei, Onate (2005)] have presented a stabilized version of the finite point method to eliminate the ill-conditioning effect due to directional arrangement of the points. Wang and Takao [wang, Takao (2004)] have proposed an isoparametric finite point method based on the concept of local isoparametric interpolation. Wen and Hon have performed a geometrically nonlinear analysis of Reissner-Mindlin plate by using a meshless collocation method based on the smooth radial basis functions. Wu, Chiu and Wang [Wu, Chiu, Wang (2008)] have developed a mesh-free col-

location method based on differential reproducing kernel approximations for the three-dimensional analysis of simply-supported, doubly curved functionally graded magneto-electro-elastic shells under the mechanical load, electric displacement and magnetic flux. Yang et al. [Yang et al. (2008)] have introduced a computational procedure based on meshless generalized finite difference method and serial magnetic resonance imaging data to quantify patient-specific carotid atherosclerotic plaque growth functions and simulate plaque progression. Zhang et al. [Zang et al. (2001)] have proposed a least-squares collocation meshless method, in which the equilibrium conditions are satisfied not only at the collocation points but also at the auxiliary points in a least-squares sense.

While, the robustness of the PCM is an issue especially when scattered and random points are used. To improve the robustness of the PCMs, Nayroles, Touzot and Villon [Nayroles, Touzot, Villon (1992)] suggested that the positivity conditions could be important when using the PCMs. Jin, Li and Aluru [Jin, Li, Aluru (2004)] have proposed techniques, based on modification of weighting functions, to ensure satisfaction of positivity conditions when using a scattered set of points. For boundary points, however, the positivity conditions cannot be satisfied, obviously, so that it is possible to get large numerical errors from the boundary points when using the PCMs. Specifically, the errors could arise in point collocation analyses with complicated boundary conditions.

In the classical moving least-square (MLS) approximation, the shape functions have no Kronecker-delta property, so that the essential node condition cannot be imposed on boundaries or on surfaces between domains using PCM and those using finite element method (FEM). In this paper, a modified MLS approximation is proposed, its shape functions have Kronecker-delta property. Therefore, the unsatisfactory issue of the essential node condition can be avoided in the modified MLS approximation. In addition, a local coordinate system is used, it renders the shape function and its derivatives of collocated points very simple.

Metal forming problems used to be analyzed by the conventional rigid-plastic finite element methods. But the conventional rigid-plastic finite element methods have some shortcomings as follows: 1) Mesh generation is needed, which is costly. 2) Remeshing is needed when deformation is appreciable, while remeshing results in loss of accuracy.

In this paper, for analyses of the rigid-plastic metal forming problems, a hybrid PCM/FEM is presented. By introducing a boundary layer of finite element in boundary domain of workpiece, unsatisfactory issue of the positivity conditions of boundary points can be avoided, and the complicated boundary conditions can be easily imposed with the boundary layer of finite element. A plane strain upsetting process is analyzed by using the hybrid PCM/FEM.

2 Formulations

Let us assume a scalar problem governed by a partial differential equation:

$$D(u) = b, \quad \text{in } \Omega \quad (1)$$

with boundary conditions

$$T(u) = t, \quad \text{on } \Gamma_t \quad (2)$$

$$u - u_c = 0, \quad \text{on } \Gamma_u \quad (3)$$

to be satisfied in a domain Ω with boundary $\Gamma = \Gamma_t \cup \Gamma_u$, where D and T are appropriate differential operators, u is the problem unknown function, b and t are external forces or sources acting over Ω and along Γ_t , respectively. u_c is the assigned value of u over Γ_u .

Let us assume Ω is divided into two subdomains, the interior domain Ω_{in} and the boundary domain Ω_{bo} . Surface between Ω_{in} and Ω_{bo} is defined as S (see Fig. 1).

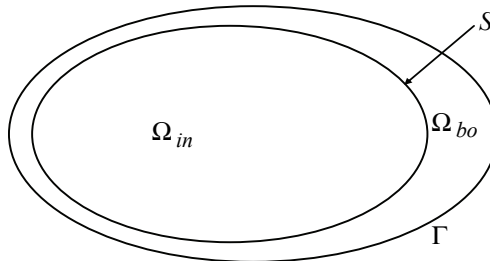


Figure 1: Interior domain Ω_{in} , boundary domain Ω_{bo} , surface S and boundary Γ

2.1 The MLS approximation with Kronecker-delta property

Consider a small domain Ω_x , the neighborhood of a point x_1 , which is located in Ω_{in} . Over Ω_x , u can be approximated by the MLS approximation. The MLS approximation with quadratic basis is not sensitive to the number of nodes in a sub-domain [Onate et al. (1996a)]. Derivatives of interpolations using the MLS approximation show smaller oscillations than those in the partition of unity method, [Atluri, Kim, Cho (1999)]. The MLS approximation has better efficiency than the radial basis point interpolation method [Liu, Gu (2003)].

Over a number of randomly located nodes $\{x_i\}$, $i = 1, 2, \dots, n$, the MLS approximation u^h of u can be defined by

$$u^h = \mathbf{p}^T(\mathbf{x}) \boldsymbol{\alpha}, \quad \forall \mathbf{x} \in \Omega_x \tag{4}$$

where $\mathbf{p}^T(\mathbf{x}) = [p_1(\mathbf{x}) \ p_2(\mathbf{x}) \ \dots \ p_m(\mathbf{x})]$ is a complete monomial basis of order m which is a function of the space coordinates $\mathbf{x} = [x \ y \ z]^T$. $\boldsymbol{\alpha}$ is a vector of unknown polynomial coefficients.

$$\boldsymbol{\alpha} = [\alpha_1 \ \alpha_2 \ \dots \ \alpha_m]^T \tag{5}$$

For example, for a 2-D problem,

$$\mathbf{p}^T(\mathbf{x}) = [1 \ x \ y \ x^2 \ xy \ y^2] \tag{6}$$

this is a quadratic basis, and $m=6$.

A weighted least-square solution is obtained for $\boldsymbol{\alpha}$ from the following system of n equations in m unknown (n is larger than m):

$$\mathbf{u}^h = \mathbf{H}\boldsymbol{\alpha} \tag{7}$$

where

$$\mathbf{u}^h = [u_1^h \ u_2^h \ \dots \ u_n^h]^T \tag{8}$$

is a vector of the nodal MLS approximation of function u , and

$$\mathbf{H} = \begin{bmatrix} \mathbf{p}^T(\mathbf{x}_1) \\ \mathbf{p}^T(\mathbf{x}_2) \\ \vdots \\ \mathbf{p}^T(\mathbf{x}_n) \end{bmatrix}_{n \times m} \tag{9}$$

The classical least-square solution of the above over-constrained system does not guarantee exact satisfaction of any of the equations of Eq. 7. Non-satisfaction of the first equation would then mean $u_1^h \neq \mathbf{p}^T(\mathbf{x}_1) \boldsymbol{\alpha}$, which, in turn, means that the least-square interpolant at node 1 is not equal to value of the node. Hence, a different approach to weighted least-squares solution can be adopted: Out of the n equations of Eq. 7, let the first equation (corresponding to node 1) be satisfied exactly and the rest in the least-square sense. This is done by using the first equation to eliminate α_1 from the rest of equations:

$$\alpha_1 = u_1^h - (\alpha_2 x_1 + \alpha_3 y_1 + \alpha_4 x_1^2 + \alpha_5 x_1 y_1 + \alpha_6 y_1^2) \tag{10}$$

Substituting for α_1 in Eq. 7, the reduced system of equations can be obtained:

$$\bar{\mathbf{u}}^h = \bar{\mathbf{H}}\bar{\boldsymbol{\alpha}} \tag{11}$$

where

$$\bar{\mathbf{u}}^h = [u_2^h - u_1^h \quad u_3^h - u_1^h \quad \cdots \quad u_n^h - u_1^h]^T \tag{12}$$

$$\bar{\mathbf{H}} = \begin{bmatrix} x_2 - x_1 & y_2 - y_1 & x_2^2 - x_1^2 & x_2 y_2 - x_1 y_1 & y_2^2 - y_1^2 \\ x_3 - x_1 & y_3 - y_1 & x_3^2 - x_1^2 & x_3 y_3 - x_1 y_1 & y_3^2 - y_1^2 \\ \vdots & \vdots & \vdots & \vdots & \vdots \\ x_n - x_1 & y_n - y_1 & x_n^2 - x_1^2 & x_n y_n - x_1 y_1 & y_n^2 - y_1^2 \end{bmatrix} = \begin{bmatrix} \bar{\mathbf{p}}^T(\mathbf{x}_2) \\ \bar{\mathbf{p}}^T(\mathbf{x}_3) \\ \vdots \\ \bar{\mathbf{p}}^T(\mathbf{x}_n) \end{bmatrix} \tag{13}$$

$$\bar{\boldsymbol{\alpha}} = [\alpha_2 \quad \alpha_3 \quad \cdots \quad \alpha_m]^T \tag{14}$$

The coefficient vector $\bar{\boldsymbol{\alpha}}$ is determined by minimizing a weighted discrete L_2 norm, defined as:

$$J = \sum_{i=2}^n w(\mathbf{x}_i) [\bar{\mathbf{p}}^T(\mathbf{x}_i)\bar{\boldsymbol{\alpha}} - \bar{u}_i]^2 = [\bar{\mathbf{H}}\bar{\boldsymbol{\alpha}} - \bar{\mathbf{u}}]^T \mathbf{W} [\bar{\mathbf{H}}\bar{\boldsymbol{\alpha}} - \bar{\mathbf{u}}] \tag{15}$$

where $w(\mathbf{x})$ is the weight function, with $w(\mathbf{x}) > 0$ for all nodes in the support of $w(\mathbf{x})$ (the support is considered to be equal to Ω_x in this paper), \mathbf{x}_i denotes the value of \mathbf{x} at node i , and the matrices \mathbf{W} is defined as

$$\mathbf{W} = \begin{bmatrix} w(\mathbf{x}_2) & 0 & \cdots & 0 \\ 0 & w(\mathbf{x}_3) & \cdots & 0 \\ \cdots & \cdots & \cdots & \cdots \\ 0 & 0 & \cdots & w(\mathbf{x}_n) \end{bmatrix}_{(n-1) \times (n-1)} \tag{16}$$

$$\bar{u}_i = \hat{u}_i - \hat{u}_1, \quad i = 2, 3, \dots, n \tag{17}$$

and

$$\bar{\mathbf{u}} = [\hat{u}_2 - \hat{u}_1 \quad \hat{u}_3 - \hat{u}_1 \quad \cdots \quad \hat{u}_n - \hat{u}_1]^T \tag{18}$$

where $\hat{u}_i, i = 1, 2, \dots, n$ are the fictitious nodal values of the function u .

Minimizing J in Eq. 15 with respect to $\bar{\boldsymbol{\alpha}}$ yields

$$\bar{\boldsymbol{\alpha}} = \mathbf{A}^{-1} \mathbf{B}\bar{\mathbf{u}} \tag{19}$$

where

$$\mathbf{B} = \bar{\mathbf{H}}^T \mathbf{W} \tag{20}$$

$$\mathbf{A} = \mathbf{B}\bar{\mathbf{H}} \quad (21)$$

Substituting Eq. 19 into Eq. 11 gives a relation which may be written as the form of an interpolation function, as

$$\bar{\mathbf{u}}^h = \bar{\mathbf{H}}\mathbf{A}^{-1}\mathbf{B}\bar{\mathbf{u}} \quad (22)$$

Eq. 10 can be rewritten as:

$$\alpha_1 = u_1^h - \mathbf{s}(\mathbf{x}_1)\bar{\boldsymbol{\alpha}} \quad (23)$$

where

$$\mathbf{s}(\mathbf{x}_1) = [x_1 \quad y_1 \quad x_1^2 \quad x_1y_1 \quad y_1^2] \quad (24)$$

Eq. 4 can be written as:

$$u^h = \alpha_1 + \mathbf{s}(\mathbf{x})\bar{\boldsymbol{\alpha}} \quad (25)$$

where

$$\mathbf{s}(\mathbf{x}) = [x \quad y \quad x^2 \quad xy \quad y^2] \quad (26)$$

Substituting Eq. 19 and Eq. 23 into Eq. 25, the following equation can be obtained:

$$u^h = u_1^h + \mathbf{q}(\mathbf{x})\mathbf{A}^{-1}\mathbf{B}\bar{\mathbf{u}} \quad (27)$$

where

$$\mathbf{q}(\mathbf{x}) = \mathbf{s}(\mathbf{x}) - \mathbf{s}(\mathbf{x}_1) \quad (28)$$

$$\mathbf{q}(\mathbf{x}_1) = \mathbf{0} \quad (29)$$

$$u^h(\mathbf{x}_1) = u_1^h \quad (30)$$

$\hat{\mathbf{u}}$ may be defined as:

$$\hat{\mathbf{u}} = [\hat{u}_1 \quad \hat{u}_2 \quad \cdots \quad \hat{u}_n]^T \quad (31)$$

then, from Eq. 27, the following equation may be obtained:

$$u^h = \mathbf{N}(\mathbf{x})\hat{\mathbf{u}} \quad (32)$$

where

$$\mathbf{N}(\mathbf{x}) = \begin{bmatrix} 1 - \left(\begin{matrix} \mathbf{q}(\mathbf{x}) & \mathbf{A}^{-1} & \mathbf{B} & \mathbf{1} \\ 1 \times (m-1) & (m-1) \times (m-1) & (m-1) \times (n-1) & (n-1) \times 1 \end{matrix} \right) \vdots \\ \begin{matrix} \mathbf{q}(\mathbf{x}) & \mathbf{A}^{-1} & \mathbf{B} \\ 1 \times (m-1) & (m-1) \times (m-1) & (m-1) \times (n-1) \end{matrix} \end{bmatrix} \quad (33)$$

In Eq. 33, $\mathbf{1}$ is vector of dimension (n-1) with all entries being equal to unity.

Recall from Eq. 29, using this result in Eq. 33, the Kronecker-delta property of $\mathbf{N}(\mathbf{x})$ may be established:

$$\mathbf{N}(\mathbf{x}_1) = [1 \quad 0 \quad 0 \quad \dots \quad 0] \quad (34)$$

which means that at node 1, the shape function for node 1 takes a value of unity and all other shape function take zero values. Therefore, Eq. 33 is the shape functions of the MLS approximation with Kronecker-delta property.

From Eq. 32 and Eq. 30, the following result can be obtained:

$$\hat{u}_1 = u^h(\mathbf{x}_1) = u_1^h \quad (35)$$

In this paper, the weight functions $w(\mathbf{x})$ may use a spline function as follows:

$$w(\mathbf{x}) = 1 - 6 \left(\frac{d}{r}\right)^2 + 8 \left(\frac{d}{r}\right)^3 - 3 \left(\frac{d}{r}\right)^4, \quad 0 \leq d \leq r \quad (36a)$$

$$w(\mathbf{x}) = 0, \quad d \geq r \quad (36b)$$

where $d = |\mathbf{x} - \mathbf{x}_1|$ is the distance from point x to the center node x_1 , and r is the radius of Ω_x , which is taken as a circle for a 2-D problem and its center is the point x_1 .

2.2 The local coordinate system

As anisotropy of the point distribution in Ω_x , matrix \mathbf{A} in Eq. 21 becomes ill-conditioned and the quality of the approximation deteriorates. In order to prevent such undesirable effect, a local coordinate system ξ, η is chosen with origin at the node x_1 for a 2-D problem, see [Boroomand, Tabatabaei, Onate (2005)],

$$\xi = \frac{x - x_1}{R_x} \quad (37a)$$

$$\eta = \frac{y - y_1}{R_y} \quad (37b)$$

where R_x and R_y denote maximum distances along x and y measured from the point x_1 to exterior nodes in Ω_x . In Eq. 36a, the spline function has now the following form in terms of the local coordinates:

$$w(\boldsymbol{\xi}) = 1 - 6 \left(\frac{\xi^2 + \eta^2}{\rho^2} \right) + 8 \left(\frac{\xi^2 + \eta^2}{\rho^2} \right)^{\frac{3}{2}} - 3 \left(\frac{\xi^2 + \eta^2}{\rho^2} \right)^2 \tag{38}$$

$\rho = 6$ is used in this paper and as usual $-1 \leq \xi \leq 1, -1 \leq \eta \leq 1$.

The matrix \mathbf{A} is not longer dependent on the dimensions of Ω_x . The approximate function is also expressed in terms of the local coordinates as

$$u^h(\boldsymbol{\xi}) = \mathbf{N}(\boldsymbol{\xi}) \hat{\mathbf{u}} \tag{39}$$

$\mathbf{A}^{-1}\mathbf{B}$ in Eq. 33 can be defined as \mathbf{C} :

$$\mathbf{C} = \mathbf{A}^{-1}\mathbf{B} \tag{40}$$

Then, from Eq. 33, entries of $\mathbf{N}(\mathbf{x})$ for the quadratic basis ($m=6$) can be written as:

$$N_1(\mathbf{x}) = 1 - \left[(x - x_1) \sum_{i=1}^{n-1} C_{1i} + (y - y_1) \sum_{i=1}^{n-1} C_{2i} + (x^2 - x_1^2) \sum_{i=1}^{n-1} C_{3i} + (xy - x_1y_1) \sum_{i=1}^{n-1} C_{4i} + (y^2 - y_1^2) \sum_{i=1}^{n-1} C_{5i} \right] \tag{41}$$

$$N_{i+1}(\mathbf{x}) = (x - x_1) C_{1i} + (y - y_1) C_{2i} + (x^2 - x_1^2) C_{3i} + (xy - x_1y_1) C_{4i} + (y^2 - y_1^2) C_{5i} \quad (i = 1, 2, \dots, n - 1) \tag{42}$$

where $C_{ji}, (j = 1, 2, \dots, 5; i = 1, 2, \dots, n - 1)$ are entries of \mathbf{C} .

At the point x_1 , because $\xi_1 = 0, \eta_1 = 0$, then the first-order derivatives of the shape function with the local coordinates can be obtained from Eqs. 41 and 42:

$$\frac{\partial \mathbf{N}(\boldsymbol{\xi}_1)}{\partial \xi} = \left[- \sum_{i=1}^{n-1} C_{1i} \quad C_{11} \quad C_{12} \quad \dots \quad C_{1(n-1)} \right] \tag{43}$$

$$\frac{\partial \mathbf{N}(\boldsymbol{\xi}_1)}{\partial \eta} = \left[- \sum_{i=1}^{n-1} C_{2i} \quad C_{21} \quad C_{22} \quad \dots \quad C_{2(n-1)} \right] \tag{44}$$

From Eqs. 43 and 44, we may see that formulas of the shape function derivatives with the local coordinates are very simple, and in fact, it is a merit of the above-mentioned PCM using the local coordinates.

2.3 The weighted residual method

Over Ω_{in} , the following weighted residual method is used:

$$\int_{\Omega_{in}} \hat{w}_i (D(\hat{\mathbf{u}}) - b) d\Omega = 0 \quad (45)$$

where \hat{w}_i is a weight function, and may be defined as follow in this paper.

$$\hat{w}_i = \delta_i \quad (46)$$

where δ_i is Dirac δ function.

Substituting Eq. 46 into Eq. 45, the following equation is obtained:

$$D(\hat{\mathbf{u}}) - b = 0 \quad (47)$$

The boundary conditions of Eqs. 2 and 3 are imposed by using the rigid-plastic FEM.

2.4 The positivity conditions

The positivity conditions on the approximation function $N_i(\mathbf{x})$ of Eq. 33 and its second-order derivatives are stated as [Jin, Li, Aluru (2004)],

$$N_i(\mathbf{x}_j) \geq 0 \quad (48)$$

$$\nabla^2 N_i(\mathbf{x}_j) \geq 0, \quad j \neq i \quad (49)$$

$$\nabla^2 N_i(\mathbf{x}_i) < 0 \quad (50)$$

where $N_i(\mathbf{x}_j)$ is the approximation function of a point i evaluated at a point j .

Patankar [Patankar (1980)] included the positivity conditions in a series of basic rules for the construction of finite differences and pointed out that the consequence of violating the positivity conditions give a physically unrealistic solution. It has been shown that the satisfaction of the positivity conditions ensures the convergence of the finite difference method with arbitrary irregular meshes for some class of elliptic problems [Demkowicz, Karafilt, Liszka (1984)]. It has been shown that the significance of the positivity conditions in meshless collocation approaches, and violation of the positivity conditions can significantly result in a large error in the numerical solution [Jin, Li, Aluru (2004)].

For a boundary point, a neighborhood centered on the point cannot be defined, so the positivity conditions on the boundary point cannot be satisfied, obviously. But for point x_1 on S , because it is not a boundary point, a small domain Ω_x , the neighborhood of the point x_1 , can be defined. Therefore, the unsatisfactory issue of the positivity conditions of boundary points can be avoided in the hybrid PCM/FEM.

2.5 The rigid-plastic hybrid PCM/FEM

For a plane strain metal forming problem, the partial differential equations of mechanical equilibrium can be expressed as (in this paper, the body forces are omitted for simplicity):

$$\frac{\partial \sigma_{11}}{\partial x} + \frac{\partial \sigma_{12}}{\partial y} = 0 \quad (51a)$$

$$\frac{\partial \sigma_{12}}{\partial x} + \frac{\partial \sigma_{22}}{\partial y} = 0 \quad (51b)$$

where σ_{11} , σ_{22} and σ_{12} are stress components. By the concept referring originally to a (nonlinear) viscous solid, the relating equation of stress vector and strain rate vector can be written as:

$$\boldsymbol{\sigma} = \mathbf{E} \dot{\boldsymbol{\epsilon}} \quad (52)$$

where

$$\boldsymbol{\sigma} = [\sigma_{11} \ \sigma_{22} \ \sigma_{12}]^T \quad (53)$$

$$\dot{\boldsymbol{\epsilon}} = [\dot{\epsilon}_{11} \ \dot{\epsilon}_{22} \ \dot{\gamma}_{12}]^T \quad (54)$$

for the rigid-plastic material

$$\mathbf{E} = \frac{\sigma_e}{\dot{\epsilon}_e} \frac{1}{3} \begin{bmatrix} 2 & 0 & 0 \\ 0 & 2 & 0 \\ 0 & 0 & 1 \end{bmatrix} + \left(\frac{1}{g} - \frac{2}{9} \right) \begin{bmatrix} 1 & 1 & 0 \\ 1 & 1 & 0 \\ 0 & 0 & 0 \end{bmatrix} \quad (55)$$

where σ_e and $\dot{\epsilon}_e$ denote the equivalent stress and the equivalent strain rate, respectively, and g is a material constant and a function of material density for slightly compressible materials.

Substituting the relationship equation of velocity and strain rate into Eq. 52, and then Eqs. 51a and 51b, the following non-linear equation of the mechanical equilibrium is derived:

$$\nabla^2 \mathbf{u} + \mathbf{f} = \mathbf{0} \quad (56)$$

in which \mathbf{u} is the velocity vector:

$$\mathbf{u} = [u \ v]^T \quad (57)$$

where u and v denote velocity components.

$$\mathbf{f} = [f_1 \ f_2]^T \quad (58)$$

where

$$f_1 = \left(\frac{3}{g} + \frac{1}{3}\right) \frac{\partial \dot{\epsilon}_v}{\partial x} + \left(\frac{1}{\sigma_e} \frac{\partial \sigma_e}{\partial x} - \frac{1}{\dot{\epsilon}_e} \frac{\partial \dot{\epsilon}_e}{\partial x}\right) \cdot \left[2\dot{\epsilon}_{11} + \left(\frac{3}{g} - \frac{2}{3}\right) \dot{\epsilon}_v\right] + \left(\frac{1}{\sigma_e} \frac{\partial \sigma_e}{\partial y} - \frac{1}{\dot{\epsilon}_e} \frac{\partial \dot{\epsilon}_e}{\partial y}\right) \dot{\gamma}_{12} \quad (59a)$$

$$f_2 = \left(\frac{3}{g} + \frac{1}{3}\right) \frac{\partial \dot{\epsilon}_v}{\partial y} + \left(\frac{1}{\sigma_e} \frac{\partial \sigma_e}{\partial y} - \frac{1}{\dot{\epsilon}_e} \frac{\partial \dot{\epsilon}_e}{\partial y}\right) \cdot \left[2\dot{\epsilon}_{22} + \left(\frac{3}{g} - \frac{2}{3}\right) \dot{\epsilon}_v\right] + \left(\frac{1}{\sigma_e} \frac{\partial \sigma_e}{\partial x} - \frac{1}{\dot{\epsilon}_e} \frac{\partial \dot{\epsilon}_e}{\partial x}\right) \dot{\gamma}_{12} \quad (59b)$$

$\dot{\epsilon}_v$ is the volumetric strain rate.

Over Ω_{in} , by the MLS approximation, \mathbf{u} in Eq. 56 can be written as:

$$u = \mathbf{N}\hat{\mathbf{u}} \quad (60a)$$

$$v = \mathbf{N}\hat{\mathbf{v}} \quad (60b)$$

Substituting Eq. 56 into Eq. 47, the partial differential equations on the nodal velocity components may be obtained:

$$\nabla^2 \mathbf{N}\hat{\mathbf{u}} + \mathbf{f}(\hat{\mathbf{u}}, \hat{\mathbf{v}}) = 0 \quad (61a)$$

$$\nabla^2 \mathbf{N}\hat{\mathbf{v}} + \mathbf{f}(\hat{\mathbf{u}}, \hat{\mathbf{v}}) = 0 \quad (61b)$$

In Ω_{bo} , the rigid-plastic FEM with one layer of finite element is used, and the boundary conditions of the metal forming problem are imposed on Γ by using the rigid-plastic FEM, too.

3 Analyzed Results of the Metal Forming Process

In this section, a plane strain upsetting problem (initial aspect ratio=1) is analyzed by using the rigid-plastic hybrid PCM/FEM. Material constant g is taken as 0.03. The friction factor is taken as 0.2. Upsetting increment is taken as 2%. The MLS approximation with the quadratic basis ($m=6$) is used. The nodal number n is taken as 9 in the PCM, and 4-noded quadratic finite element are adopted in the FEM. The flow-stress-characteristics data of the material is given by the expression,

$$\sigma_e = 589.86\epsilon_e^{0.0625} \text{ MPa}, (\epsilon_e \geq 0.002) \quad (62a)$$

$$\sigma_e = 400 \text{ MPa}, (\epsilon_e \leq 0.002) \quad (62b)$$

where ϵ_e denotes the equivalent strain.

Figs. 2 and 3 show fields of the nodal velocity at 30% reduction and 50% reduction, respectively, and only one quadrant the of the workpiece is calculated owing to symmetry.

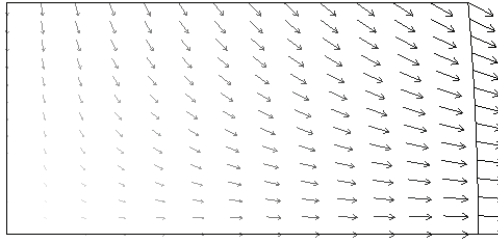


Figure 2: Nodal velocity field at 30% reduction

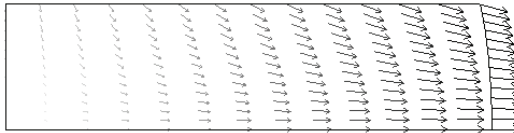


Figure 3: Nodal velocity field at 50% reduction

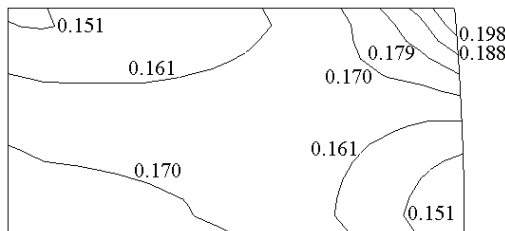


Figure 4: Contours of equivalent strain rate (1/s) at 30% reduction

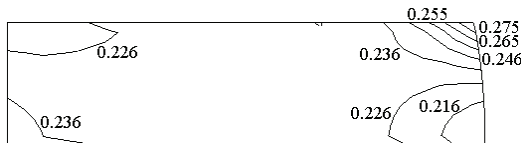


Figure 5: Contours of equivalent strain rate (1/s) at 50% reduction

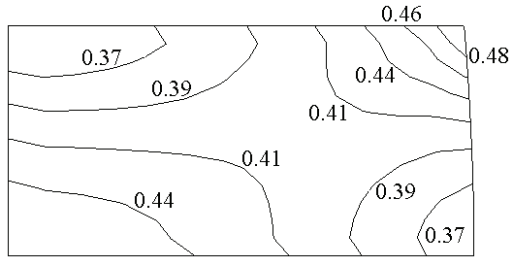


Figure 6: Contours of equivalent strain at 30% reduction

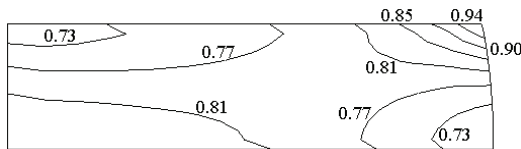


Figure 7: Contours of equivalent strain at 50% reduction

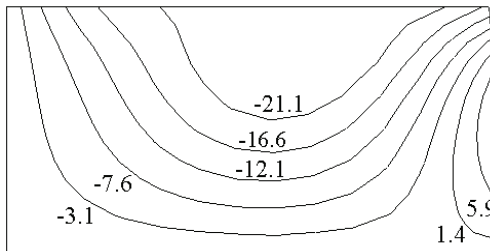


Figure 8: Contours of shear stress (MPa) at 30% reduction

Figs. 4 and 5 show contours of equivalent strain rate at 30% reduction and 50% reduction, respectively. As seen in these figures, the equivalent strain rates of the corners and the center are larger, and those of the center end zones and the center free boundary zones are smaller, at both the reduction cases.

Figs. 6 and 7 show contours of equivalent strain at 30% reduction and 50% reduction, respectively. As seen in these figures and Figs. 4 and 5, the distributions of the equivalent strain are similar to that of the equivalent strain rate, the equivalent strains of the corners and the center are larger, and those of the center end zones and the center free boundary zones are smaller.

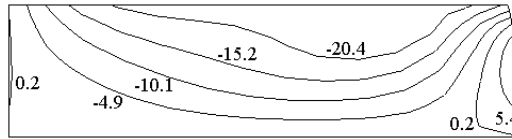


Figure 9: Contours of shear stress (MPa) at 50% reduction

Figs. 8 and 9 show contours of shear stress at 30% reduction and 50% reduction, respectively. As seen in these figures, values of the shear stresses of the middle end zones are larger, and those near to the two symmetry lines and the free boundaries are smaller. values of the shear stresses of the corners change sharply, and directions of these shear stresses vary.

4 Conclusions

In some PCMs, the positivity conditions of boundary points cannot be satisfied, so that it is possible to get large numerical errors from the boundary points. Specifically, the errors could arise in the analyses of metal forming problems which have complicated boundary conditions. By introducing a boundary layer of finite element in boundary domain of analyzed body, unsatisfactory issue of the positivity conditions of boundary points in the PCMs can be avoided, and the complicated boundary conditions can be easily imposed with the boundary layer of finite element. By making such an improvement, the hybrid PCM/FEM can be used for analyzing problems of metal forming effectively.

In addition, the modified MLS approximation is proposed in this paper, its shape functions have Kronecker-delta property. Then, the unsatisfactory issue of the essential node condition of the classical MLS approximation can be avoided in the modified MLS approximation.

References

- Aluru, N. R.** (2000): A point collocation method based on reproducing kernel approximations. *Int. J. Numer. Methods Engrg.*, vol. 47, pp. 1083-1121.
- Atluri, S. N.; Zhu, T.** (1998): A new meshless local Petrov-Galerkin (MLPG) approach in computational mechanics. *Computational Mechanics*, vol.22, pp. 117-127.
- Atluri, S. N.; Kim, H. G.; Cho, J.Y.** (1999): A critical assessment of the truly meshless local Petrov-Galerkin (MLPG), and local boundary integral equation (LBIE) methods. *Computational Mechanics*, vol. 24, pp. 348-372.

Atluri, S. N.; Liu, H. T.; Han, Z. D. (2006a): Meshless local Petrov-Galerkin (MPLG) mixed collocation method for elasticity problems. *CMES: Computer Modeling in Engineering & Sciences*, vol. 14, pp. 141-152.

Atluri, S. N.; Liu, H. T.; Han, Z. D. (2006b): Meshless local Petrov-Galerkin (MPLG) mixed finite difference method for solid mechanics. *CMES: Computer Modeling in Engineering & Sciences*, vol. 15, pp. 1-16.

Belytschko, T.; Lu, Y. Y.; Gu, L. (1994): Element free Galerkin methods. *Int. J. Numer. Methods Engrg.*, vol. 37, pp. 229-256.

Boroomand, B.; Tabatabaei, A. A.; Onate, E. (2005): Simple modifications for stabilization of the finite point method. *Int. J. Numer. Methods Engrg.*, vol. 63, pp. 351-379.

Chantasiriwan, S. (2006): Performance of multiquadric collocation method in solving lid-driven cavity flow problem with low Reynolds number. *CMES: Computer Modeling in Engineering & Sciences*, vol. 15, pp. 137-146.

Demkowicz, L.; Karafil, A.; Liszka, T. (1984): On some convergence results for FDM with irregular mesh. *Comput. Methods Appl. Mech. Engrg.*, vol. 42, pp. 343-355.

Duarte, C. A.; Oden, J. T. (1996): An h-p adaptive method using clouds. *Comput. Methods Appl. Mech. Engrg.*, vol. 139, pp. 237-262.

Jin, X.; Li, G.; Aluru, N. R. (2004): Positivity conditions in meshless collocation methods. *Comput. Methods Appl. Mech. Engrg.*, vol. 193, pp. 1171-1202.

Kosec, G.; Sarler, B. (2008): Local RBF collocation method for Darcy flow. *CMES: Computer Modeling in Engineering & Sciences*, vol. 25, pp. 197-207.

Li, S.; Atluri, S. N. (2008a): Topology-optimization of structures based on the MPLG mixed collocation method. *CMES: Computer Modeling in Engineering & Sciences*, vol. 26, pp. 61-74.

Li, S.; Atluri, S. N. (2008b): The MPLG mixed collocation method for material orientation and topology optimization of anisotropic solids and structures. *CMES: Computer Modeling in Engineering & Sciences*, vol. 30, pp. 37-56.

Liu, G. R.; Gu, Y. T. (2003): A meshfree method: meshfree weak-strong (MWS) form method, for 2-D solids. *Computational Mechanics*, vol. 33, pp. 2-14.

Liu, W. K.; Jun, S.; Li, S.; Adee, J.; Belytschko, T. (1995): Reproducing kernel particle methods for structural dynamics. *Int. J. Numer. Methods Engrg.*, vol. 38, pp. 1655-1679.

Melenk, J. M.; Babuska, I. (1996): The partition of unity finite element method: basic theory and applications. *Comput. Methods Appl. Mech. Engrg.*, vol. 139, pp. 289-314.

Nayroles, B.; Touzot, G.; Villon, P. (1992): Generalizing the FEM: diffuse approximation and diffuse elements. *Computational Mechanics*, vol. 10, pp. 307-318.

Onate, E.; Idelsohn, S.; Zienkiewicz, O. C.; Taylor, R. L. (1996a): A finite point method in computational mechanics. Applications to convective transport and fluid flow. *Int. J. Numer. Methods Engrg.*, vol. 39, pp. 3839-3866.

Onate, E.; Idelsohn, S.; Zienkiewicz, O. C.; Taylor, R. L.; Sacco, C. (1996b): A stabilized finite point method for analysis of fluid mechanics problems. *Comput. Methods Appl. Mech. Engrg.*, vol. 139, pp. 315-346.

Patanakar, S. V. (1980): *Numerical Heat Transfer and Fluid Flow*, Hemisphere.

Wang, W. X.; Takao, Y. (2004): Isoparametric finite point method in computational mechanics. *Computational Mechanics*, vol. 33, pp. 481-490.

Wen, P. H.; Hon, Y. C. (2007): Geometrically nonlinear analysis of Reissner-Mindlin Plate by meshless computation. *CMES: Computer Modeling in Engineering & Sciences*, vol. 21, pp. 177-191.

Wu, C.-P.; Chiu, K.-H.; Wang, Y.-M. (2008): A mesh-free DRK-based collocation method for the coupled analysis of functionally graded magneto-electro-elastic shells and plates. *CMES: Computer Modeling in Engineering & Sciences*, vol. 35, pp. 181-214.

Wu, X.-H.; Shen, S.-P.; Tao, W.-Q. (2007): Meshless local Petrov-Galerkin collocation method for two-dimensional heat conduction problems. *CMES: Computer Modeling in Engineering & Sciences*, vol. 22, pp. 65-76.

Yang, C.; Tang, D.; Yuan, C.; Kerwin, W.; Liu, F.; Canton, G.; Hatsukami, T. S.; Atluri, S. N. (2008): Meshless generalized finite difference method and human carotid atherosclerotic plaque progression simulation using multi-year MRI patient-tracking data. *CMES: Computer Modeling in Engineering & Sciences*, vol. 28, pp. 95-107.

Zhang, X.; Liu, X.-H.; Song, K.-Z.; Lu, M.-W. (2001): Least-squares collocation meshless method. *Int. J. Numer. Methods Engrg.*, vol. 51, pp. 1089-1100.

Zhu, T.; Zhang, J.; Atluri, S. N. (1998): A local boundary integral equation (LBIE) method in computational mechanics and a meshless discretization approach. *Computational Mechanics*, vol.21, pp. 223-235.

